JGR Space Physics

Key Points:

- Pitch angle distributions of electrons are used to establish field-aligned beams near Callisto from the moon-magnetosphere interaction
- Close to the moons, field-aligned electron are accelerated in regions with changing density and magnetic field to maintain the current flow
- There is evidence that at Callisto Alfvén waves could have accelerated electrons along field lines up to several hundreds of keV

Correspondence to:

N. Krupp,
krupp@mps.mpg.de

Pitch Angle Distributions of Energetic Particles Near Callisto

N. Krupp[1] , **E. Roussos**[1] , **M. Fränz**[1], **P. Kollmann**[2] , **C. Paranicas**[2] , **G. Clark**[2] , **K. Khurana**[3] , and **A. Galli**[4]

[1]Max Planck Institute for Solar System Research, Göttingen, Germany, [2]The Johns Hopkins University Applied Physics Laboratory, Laurel, MD, USA, [3]University of California Los Angeles, Los Angeles, CA, USA, [4]Physikalisches Institut, University of Bern, Bern, Switzerland

Abstract The Galileo spacecraft performed close flybys of the moon Callisto between 1996 and 2001. We reanalyzed particle data of the energetic particles detector onboard Galileo and derived pitch angle distributions in the energy range of several keV to MeV during Callisto flybys C3, C9, C10, and C30. We establish that field-aligned beams observed during the flyby periods are more likely to originate from Callisto's magnetospheric interaction rather than by independent magnetospheric processes. These beams are prominent only during flyby C3, they come mainly from the North, and connect the moon and the ionosphere of Jupiter. For short intervals they have also been observed propagating from the South. The beams are regularly unidirectional and typically extend to 300 keV in energy, occasionally reaching above 600 keV. Energetic particle depletions in Callisto's wake during the downstream flybys are not at all obvious, even at low altitudes and in the wake center. The signature of the wake becomes more apparent when energetic particle observations are organized in pitch angle. In that case, pitch angle distribution minima at 90 deg can be discerned in some flybys, however, not always associated with a profound drop in the absolute signal intensity. They instead indicate that field-aligned particle flux within the wake is higher. Outside the wake these minima continue in an energy-dependent disturbed region toward Jupiter which seems to be at least partially collocated with Alfvén-wing structures as predicted from magnetohydrodynamic simulation results or simple flyby geometry considerations.

Plain Language Summary Pitch angle distributions of energetic electrons and ions during four close Callisto encounters of the Galileo spacecraft are analyzed and clear signatures of electron beams were found only for one of the four flybys. The beam energies extend up to 300 keV at least. The origin of those beams lies in the interaction between the plasma in the Jovian magnetosphere and the exosphere of Callisto. The electron beams were observed in regions of changing density and magnetic field values where the electrons are accelerated to maintain the current flow. The acceleration itself is most probably related to Alfvén waves.

1. Interaction of Callisto With the Jovian Plasma and Energetic Particles

Understanding the moon-magnetosphere interaction (Kivelson, 2004; Kivelson et al., 2004; Simon et al., 2015) between the surrounding plasma in the magnetospheres of Jupiter and Saturn and the exosphere or surface of the moons embedded within these giant and very complex system is one of the most interesting topics in planetary plasma physics. Especially the interaction at Callisto, the outermost of the four Galilean satellites orbiting Jupiter, deeply embedded in the Jovian magnetosphere orbiting at 26.3 Jovian radii R_J (1 R_J = 71,492 km) is, compared to the corresponding interactions at Io, Europa and Ganymede, considerably less investigated. With two future spacecraft missions that will flyby the moon multiple times early in the next decade, there is a strong motivation to re-analyze existing data sets from previous Callisto in-situ observations. More specifically, the ESA-mission JUICE (JUpiter ICy moons Explorer) launched in April 2023, arriving at Jupiter in September 2031, will fly by Callisto 21 times and the NASA-mission Europa Clipper (launch planned for 2024) will reach Jupiter in 2030 and will also pass by Callisto multiple times. Both missions will carry sophisticated instrumentation to characterize the plasma environment and magnetosphere interactions of Callisto. In order to understand the interaction we need: (a) information about parameters of the local neutral, plasma and magnetic field environment of the moon itself, and (b) information about the charged particle and magnetic field conditions in the magnetosphere surrounding Callisto.

Regarding Callisto's local environment, we know that the moon possesses a considerable ionosphere with densities ranging between 100 and 400 cm^{-3} and an O_2-dominated ion composition. The ionospheric density profile

appears to vary both as a function of longitude and latitude of Callisto and as a function of Callisto's orbital location around Jupiter, the latter determining the angle between the solar illumination and the plasma ram on the moon's upstream hemisphere. For a range of parameters of Callisto's ionosphere see Gurnett et al. (1997, 2000), Kliore et al. (2002), Seufert (2012), Kivelson et al. (2004). Local magnetic field measurements by the Galileo spacecraft indicated that Callisto does not possess a global, permanent magnetic field. Instead, signatures of magnetic induction reported by Khurana et al. (1998) and Kivelson et al. (1999) showed that the moon might have a liquid water ocean underneath its thick icy crust, much like Europa and Ganymede. Besides the induction signatures, the macroscopic characteristics of additional local magnetic field disturbances by the moon's ionospheric interaction with Jupiter's magnetosphere appear consistent with those of a superalfvénic, subsonic and submagnetosonic interaction and resemble that of Titan's plasma interaction at Saturn. On the other hand, the details of these magnetic field disturbances are challenging to fully reconstruct in magnetohydrodynamic (MHD) or hybrid simulations (see Seufert (2012); Lindkvist et al. (2015); Liuzzo et al. (2015); Liuzzo et al. (2016); Liuzzo et al. (2017, 2019)), hinting that external forcing of the interaction by Jupiter's dynamic magnetospheric environment at Callisto's distance contributes to the complexity of the interaction. In the used simulations a certain set of initial conditions are used and changes of those conditions within the time period of interest are normally not taken into account. Therefore, the comparison between simulation results and the recorded data always shows differences on a certain level. The plasma and energetic charged particle populations in the magnetosphere of Jupiter, originating mainly from the innermost Galilean satellite Io, corotate around the planet and have their highest concentration within a plasma sheet configuration around the magnetic equatorial plane. The measured flow velocity values from Galileo (Krupp et al., 2001; Kane et al., 1999; Bagenal et al., 2016; Waldrop et al., 2015) and recently from Juno (Kim et al., 2020) range from 100 to 300 km/s while the rigid corotation velocity at Callisto's orbit is about 327 km/s. Callisto, which orbits Jupiter at about 8.2 km/s, is thus overtaken by the background plasma flow (Galli et al., 2022), meaning that disturbances from the magnetospheric interaction largely extend downstream of Callisto and in the direction of corotation. Callisto orbits in a region sometimes referred to as the corotation breakdown region. This is where flow velocities start to significantly deviate from rigid corotation and where field-aligned current systems arise magnetically mapping into parts of the main auroral region in Jupiter's ionosphere are thought to occur. Since the rotational and the magnetic dipole axes are separated by about 10°, the plasma sheet wobbles up and down with respect to the equatorial plane changing periodically the properties of plasma and energetic particles that impinge on Callisto. At the same time, the magnetic field orientation and strength vary accordingly, having a near south to north pointing and minimum magnitude when Callisto is close to the magnetic equator, and a much more inclined/radial orientation as Callisto is away from the plasma sheet center. The charged particle environment of the magnetosphere around Callisto is additionally highly variable due to dynamic changes in the magnetosphere of Jupiter that develop over a variety of time scales (from minutes to days) (Mauk & Saur, 2007). At Callisto the energetic ions play an important role since they provide 95% of the total pressure (Kivelson et al., 2004) and the plasma beta (ratio particle pressure/magnetic field pressure) can be as large as $\beta = 64$ at the center of the plasma sheet. The downstream region is the location where strong interaction features with the moon are expected to be seen. These may take the form of a simple wake cavity, where charged particles are partially or heavily depleted due to absorption on the moon, or a region which is filled with plasma and pick-up ion populations originating from a moon's ionized atmosphere or exosphere. The presence of the moon leads to a disturbed and decelerated plasma flow and distorted piled up field lines close to the moon while further away the plasma remains unchanged. The draped field lines form a current system and a final standing wave pattern (Alfvén-wing) builds up (for details see Kivelson and Russell (1995), Neubauer (1980), and Knight (1973)) if there is a substantial ionosphere present.

From the short review above it is clear that much of what we know about Callisto's magnetospheric interaction derives from magnetic field and ionospheric measurements, as well as from simulations. In addition, Bhattacharyya et al. (2018) reported evidence of Callisto's footprint in Jupiter's aurora analyzing Hubble Space Telescope images. Its brightness points to significant fluxes of Callisto-originating precipitating energetic field-aligned electrons. The latter is, however, only an indirect observation of Callisto's plasma interaction. Overall, excluding the descriptions of Callisto's ionosphere, the information on charged particle observations at eV-MeV energies in Callisto's local interaction region is little to none, even if we consider Juno observations. Juno observations account for a considerable progress in the description of the upstream plasma and energetic particle environment of Callisto (Kim et al. (2020)), adding to past observations by the Galileo and Voyager spacecraft, the former crossing Callisto's L-shell multiple times. However, Juno did not perform close flybys of Callisto which could inform us about the local interaction properties.

The only spacecraft that has performed dedicated Callisto flybys is Galileo. Due to the limited performance of Galileo's PLS instrument at and beyond Callisto's orbit (Frank et al., 1992), plasma observations from those flybys remain unpublished. One attempt to describe the interaction through in-situ particle measurements comes from Mauk and Saur (2007): while studying several intervals of high time and angular resolution energetic electron measurements in Galileo/energetic particles detector (EPD) data, they observed a series of intervals with highly structured and intense electron beams, related to upward and downward currents along field lines. Coincidentally, some of these beams were seen near times of Callisto flybys. However, the authors could not conclusively discern whether certain features in the data were due to Callisto or the magnetosphere. The simplest expectation of Callisto's interaction, especially in energetic particles, would have been that of reduced particle fluxes in wake region downstream (leading side) of the moon, and little to no disturbances upstream (trailing side). That would have been the case of a plasma absorbing interaction. Given, however, that Callisto is not a simple plasma and energetic particle absorber, wake features may not be too prominent. In that respect, it would be important to not just focus on time-series of charged particle fluxes during Callisto flybys, but also take into account their evolving pitch angle distributions (PADs). We notice, in particular, that Mauk and Saur (2007) limited their PAD analysis to selected electron channels of Galileo/EPD, particularly since their focus was on locating electron beams rather than analyzing the Callisto flyby data. Discerning whether the beams they observed are Callisto or magnetosphere-driven can be achieved by expanding this analysis to a larger range of particle energies as well as to different species. Overall, PADs of energetic particles are a useful tool to study the global topology of field lines, to better understand the auroral activity related to field-aligned electrons, and to identify the interaction region between a planetary magnetosphere and a moon embedded in it. For instance, Tomás et al. (2004) showed that PADs of electrons clearly showed a boundary from being trapped to being more field-aligned configuration with respect to the magnetic field between 10 and 17 R_J. The extension of this region did not show a dependence in energy. Similarly, Frank and Paterson (2002) indicated that bi-directional electron beams in PLS data at 20–30 R_J in the vicinity of Callisto's L-shell (but far from Callisto). Therefore, field-aligned PADs near the L-shell of Callisto are expected to be observed. At the same time, we could anticipate that at least those PADs' topology, if observed at different energies and species, changes depending on whether these are driven from a moon-magnetosphere interaction or from magnetosphere dynamics. Strongly localized and energy dependent evolving PADs point more to a moon-magnetosphere interaction, due to the energy-dependent disturbances that are enhanced in the energetic particle drifts (Liuzzo et al., 2019). It is also important to organize observations in pitch angle, as certain interaction features may be present only within narrow pitch angle ranges (Khurana et al., 2008). In order to better plan JUICE and Europa Clipper observations it is thus worth putting together and reanalyzing the Galileo flyby observations at Callisto, the only one to ever perform close Callisto flybys to date. During the flybys of Galileo at Callisto the transition from the magnetosphere to the moon's interaction region will be resolved mostly through the energetic particle and magnetic field measurements (EPD (Williams et al., 1992) and Galileo magnetometer/MAG (Kivelson et al., 1992)), while plasma (PLS) observations will not be considered due to their limited signal to noise characteristics, as mentioned before.

2. Data Sets Used

In this study we used the updated calibrated data from the EPD (instrument details can be found in Williams et al. (1992)) and from the magnetometer instrument MAG (more information in Kivelson et al. (1992)) onboard the Galileo spacecraft. EPD was able to measure electrons, ions and various ion species separately with two different types of sensors (LEMMS and CMS) mounted on a movable motor platform. Distinct motor positions relative to the spin axis of the spacecraft together with the spacecraft rotation enabled measurements of energetic charged particles from nearly all directions in space. Each motor position lasted for one spin of 20 s so that a full three-dimensional particle distribution could be obtained every 120 s. The measurable energy range is keV to MeV for electrons, ions, and different ion species (p, He, O, S). A summary of the subset of selected channels for electrons and ion species and for a range of energies are listed below in Table 1. Knowing the direction from more than 400 directions in space relative to the direction of the magnetic field $\vec{B}$ provided by the MAG instrument, the particle pitch angle can be derived where 0° means that the particles is moving parallel to the magnetic field and 90° means moving perpendicular to it.

3. Callisto Flybys of the Galileo Spacecraft

Galileo performed eight dedicated close Callisto flybys (C3, C9, C10, C20, C21, C22, C23, C30) and one slightly more distant, untargetted flyby following Ganymede flyby G8. Here we analyze four flybys only listed in Table 2

Table 1

Selected Energy Channels of the EPD Sensors Onboard the Galileo Spacecraft Used for This Study

Channel	Measured species	Energy range (keV)	EPD sensor
E0	Electrons	15–29	LEMMS
E1	Electrons	29–42	LEMMS
E2	Electrons	42–55	LEMMS
E3	Electrons	55–83	LEMMS
F0	Electrons	83–188	LEMMS
F1	Electrons	174–304	LEMMS
F2	Electrons	304–527	LEMMS
F3	Electrons	527–884	LEMMS
B1	Electrons	1,500–10500	LEMMS
DC2	Electrons	>2,000	LEMMS
DC3	Electrons	>11,000	LEMMS
A0	Ions	22–42	LEMMS
A2	Ions	65–120	LEMMS
A3	Ions	120–280	LEMMS
A3	Ions	280–515	LEMMS
TP1	Protons	80–220	CMS
TP2	Protons	220–540	CMS
TP3	Protons	540–1,040	CMS

Note. Some energy ranges are approximate, especially for the integral channels or for the TP-channels which have variations in their responses due to radiation damage. Much of the information is available in the user guide of EPD along with the new calibrated data set of EPD found at https://pds-ppi.igpp.ucla.edu/search/view/?f=yes&id=pds://PPI/galileo-epd-cal-corrected.

Table 2

Selected Flybys of the Galileo Spacecraft at Callisto Where Data From the EPD Instrument Are Available

Flyby	Closest approach (km)	Date (day of year)	Magnetic latitude (degrees)	Local time
C3	1,136	4 November 1996 (309)	6.78	07:48
C9	418	25 June 1997 (176)	−7.64	05:32
C10	539	17 September 1997 (259)	−6.48	05:02
C30	138	25 May 2001 (145)	−5.01	13:09

where EPD data are available and statistically relevant with sufficient time resolution to obtain the highest quality PADs. In addition, the distance of closest approach, the date and time of the flyby as well as the magnetic latitude and the local time for each flyby are listed. The trajectories of the Callisto flybys are shown in two useful coordinate systems. In Figure 1 a coordinate system is shown with Callisto in the center where x is the corotation direction of the moving plasma in the Jovian magnetosphere, y is the direction toward Jupiter and z pointing North completes the right-handed system. In Figure 2 x is also in the flow direction, z along the magnetic field direction, and y completes the right-handed system. We use both for interpreting the data. Sometimes it is better to show the trajectory in a magnetic field based coordinate system, sometimes in a more geometrically fixed system. All of those flybys crossed the geometric wake downstream behind the moon, except C9 which happened upstream from Callisto. An example of measured count rates of energetic charged particles during Callisto flyby C3 is shown in Figure 3. The measured fluxes as a function of time are shown for electrons in three different energy ranges (top panel), same for three total ion channels, mostly protons (middle panel), and for three channels measuring protons only (lower panel). Closest approach is marked by a vertical line annotated with C3. There are a few signatures in the data related to different regions crossed by the spacecraft (magnetosphere, wake, and disturbed region). Marked in yellow is the geometric wake region behind the moon relative to the magnetospheric flow in corotation direction. When Galileo entered the wake nearly all of the fluxes of electrons, ions and protons increased unlike what we would have expected: at the energies of EPD, where moon originating populations like pick-up ions are not resolvable, we would have expected to see at least partial losses. However, there is no report of a strong depletion or the detection of pick-up ions during the crossing of the wake so far. The strong electromagnetic induction from the interior and the ionosphere of Callisto and the Alfvénic interaction of the moon with the Jovian plasma shields a large fraction of the Jovian magnetic field from Callisto. This may also be the reason for the very weak loss of plasma populations in the wake of Callisto.

On top of this increase in this region we noted sharp short spikes in the electron and ion fluxes related to 0 and 180° pitch angle as shown later in more detail. After closest approach, nearly in the center of the wake, the electron fluxes show a higher degree of fluctuations. Corotational flow signatures seem to be absent or disturbed and are not clearly visible in the wake region. At the exit from the wake toward the direction of Jupiter a region with slightly more disturbed fluxes was crossed (gray shaded region), indicating that in this region the undisturbed magnetosphere without an influence of the moon was not yet reached, visible especially in electron channel B1 (1,500–10,500 keV). However, it could be noted that clear periodic flux variations are observed in the ion and proton channels with the highest fluxes when the sensor looked into the corotational flow direction. This continued when the spacecraft was back into the undisturbed magnetosphere (white background). On top of the motion of the detector more variations are visible at higher frequencies related to different look directions. The pitch angle space is sampled at a higher rate than the corotation direction, which is why the frequency of the variations due to pitch angle sampling are faster. In the magnetosphere before the wake entry and after leaving the disturbed region fewer fluctuations with smaller amplitudes were recorded in electron fluxes. The somehow limited observations are far from being clear on what corresponds to the magnetosphere and what to the Callisto interaction, which is why we need to distinguish between the different components of the observations in species, energy, and most importantly, pitch angle. For the following Figures 4 and 6–8 we plot the particle data in the coordinate system shown to Figure 1.
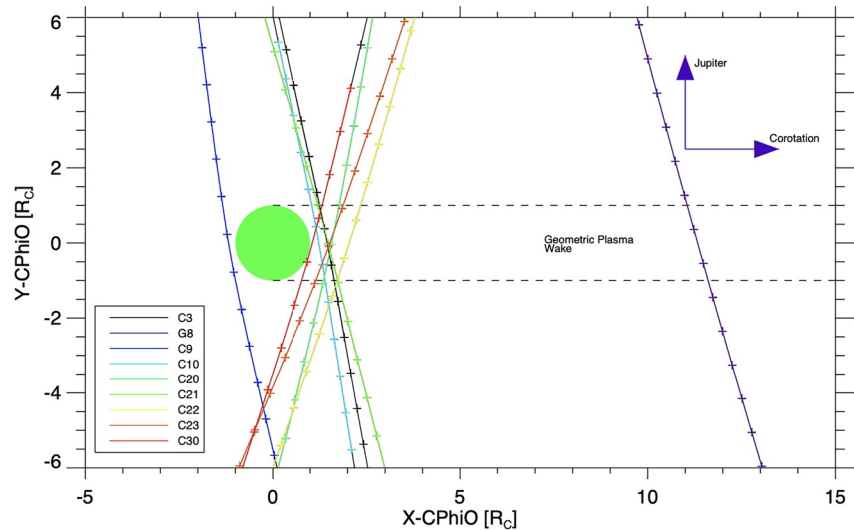
Figure 1. Trajectories of the Galileo spacecraft during all close Callisto encounters. Callisto is in the center of the coordinate system, *x* points in the flow direction, *y* toward Jupiter and *z* pointing North. Tick marks along the trajectories are 5 min apart. The units are in Callisto Radii R_C.

4. Pitch Angle Distributions of Energetic Electrons Near Callisto

The measured pitch angle distributions of electrons in channel E0 (15–29 keV) are shown in Figure 4 for flybys C3, C9, C10, and C30. For each of those flybys the spacecraft trajectory is shown in the top panel in the same coordinate system described in Figure 1 together with the measured count rates (middle panel) and the pitch angle distributions (lower panel). The dashed lines indicate the geometric wake behind the moon. Count rates and pitch angle distributions measured during the various flybys were all different:

Flyby C3: At the time of flyby the count rates were quite low compared to other flybys and the fluctuations were stronger compared to C9 or C30. At C3 the pitch angle distributions clearly indicate field-aligned electron beams with maxima at 0° pitch angle during the wake crossing marked by the circle. It is worth noting that there is one time interval after wake entry where a beam at 180° has been recorded and a few periods where bi-directional beams at 0 and 180° pitch angle (at entry and before exit of the wake) were measured. Since the Jovian magnetic field at the equator is mainly north-south, 0° pitch angle near the equatorial plane indicate a beam from the North, 180° from the South. This observation is consistent with Figure 13a of Mauk and Saur (2007) where the fitting parameter *m* indicated beams. After leaving the wake toward the direction of Jupiter significant decrease of particles (bite-outs) at 90° pitch angles were seen in the disturbed region followed by nearly isotropic distributions in the magnetosphere. Bhattacharya et al. (2005) reported electron injection events between 13:47 and 13:59 during that flyby.

Flyby C9: The flyby happened upstream of the moon and the electron pitch angle distributions were quite isotropic. Overall the count rates are higher after closest approach toward Jupiter.

Flyby C10: During this flyby 90° pitch angle depletions could be observed in the wake and in the disturbed region outside the wake. The deepest depletion is close before the exit of the wake and is also nicely visible in the fluxes. In the disturbed region after exiting the wake more dropouts but not as deep as before are observed. Gurnett et al. (2000) reported the highest ionospheric electron densities of 400 cm⁻³ of all the flybys in the wake pointing to the fact that Callisto is a significant source of plasma and Liuzzo et al. (2016) reported field line draping and associated Alfvén-wing structures as described above in a simulated flyby C10 scenario.

Flyby C30: Finally at flyby C30, which was the closest flyby of all crossing the wake at 130 km distance only, the fluxes were fairly high and isotropic and very disturbed with a few short dropouts and unclear changes in the pitch angle distributions. Generally, in wakeside flybys, the absence of a wake depletion seems to be the rule rather than the exception, at least for the electrons of 15–29 keV. C10 is the exception, still even in that case the depletion is much narrower than the moon's diameter, and not centered in the wake axis. These statements are consistent with most of the upstream magnetic flux and plasma avoiding Callisto because of its high conductivity.
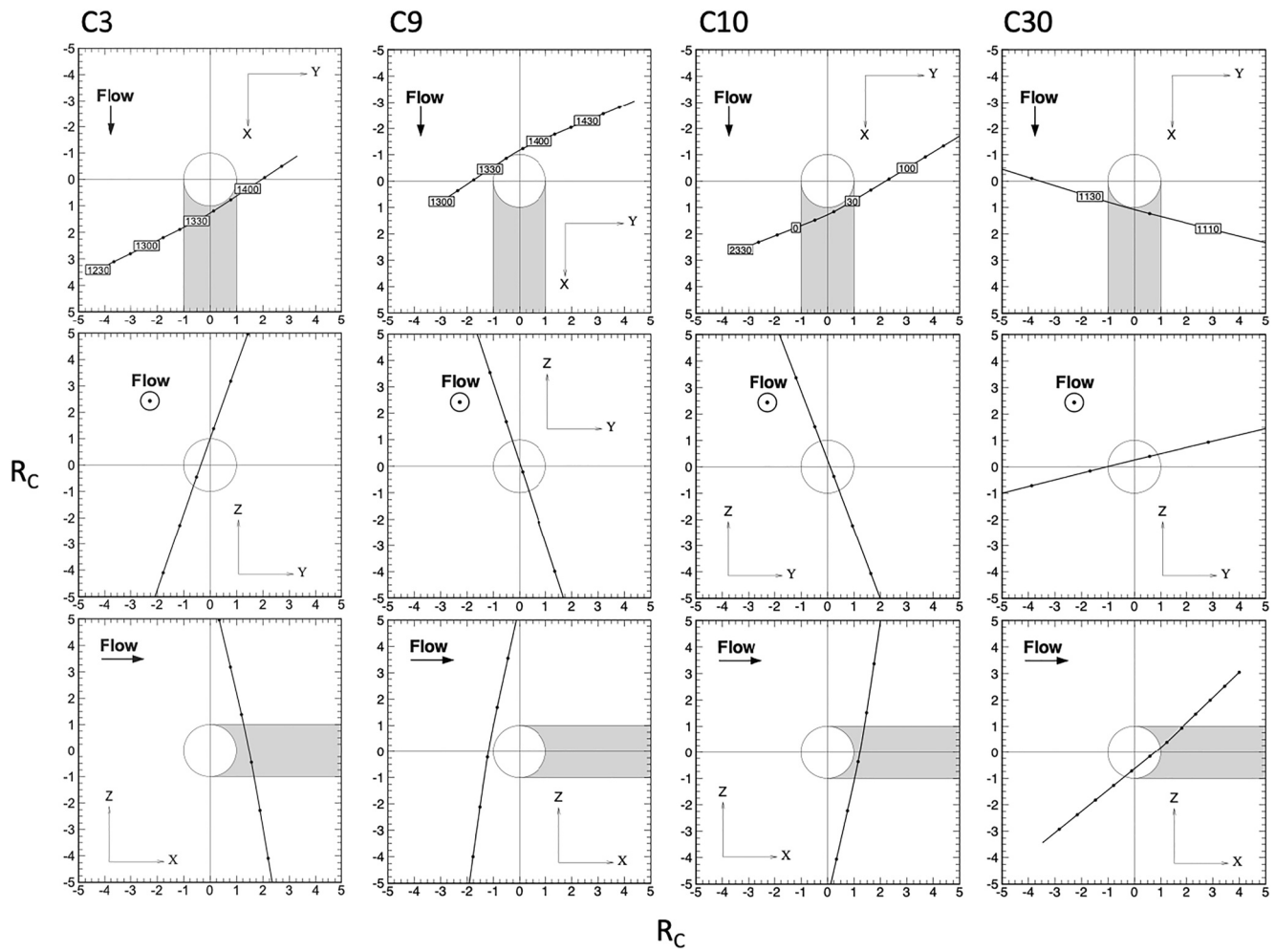
Figure 2. Trajectories of the Galileo spacecraft during Callisto encounters C3, C9, C10, and C30 in a coordinate system where Callisto is in the center, *x* points in the flow direction, *z* along the magnetic field direction and y completes the right-handed system. Time along the trajectories are labeled every 10 min. The units are in Callisto Radii R_C.

From these observations it seems that flyby C3 is somehow different compared to the other three. One possibility is that actually the spacecraft went through the Alfvén-wing during this pass. It is also the only flyby of those four where the spacecraft was on positive magnetic latitudes of 6.78° as summarized in Table 2. The other three were on slightly southern magnetic latitudes between −5.01 and −7.64°. Therefore, we investigated the field-aligned electron beams during C3 and looked at the energy dependence of those beams in more detail. The time range is 1996-309/13:20:00 to 1996-309/13:48:35. In Figure 5 we show the electron pitch angle distributions as a function of energy versus time before the wake crossing (rows 1–2); in the wake (rows 2–4) and after exiting the wake in the disturbed region (rows 4–5). Each box shows the pitch angle on the *x*-axis versus energy on the *y*-axis for a given time listed above the box. For each box we used a detrending (the actual count rate at the original time resolution is smoothed give us an estimated detrend rate = actual rate/smooth rate. The smoothing window depends on the number of data points and is carefully chosen to get the best detrending), a pitch angle binning of 10 deg, and a time step of 80 s. The color-coding is normalized to the maximum for each energy bin in each box independently. Before crossing the wake during flyby C3 the electron pitch angle versus energy distributions were quite homogeneous and the energy spectrum was quite flat. No beams were seen. The first beams were found at 13:29 from the North (o degree pitch angle) only in the energy range 29–500 keV. Electron beams with energies 300–900 keV from the South (180° pitch angle) were seen as well during that time period which means bi-directional beams between 300 and 500 keV. 120 seconds later bi-directional beams between 29 and 50 keV and beams from the South only up to 300 keV were visible. Beams with energies 29–884 keV from the North followed by beams from the South followed by beams from the North as the spacecraft crossed the wake (see rows
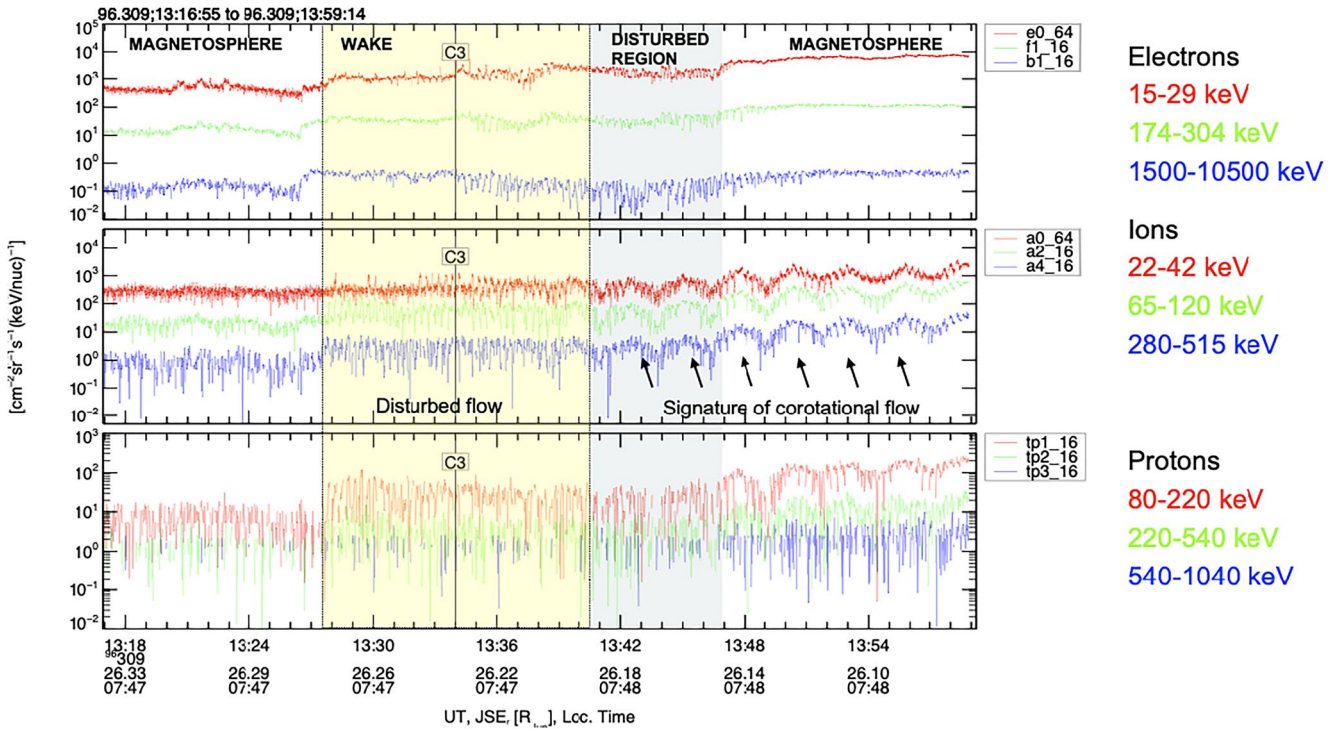
Figure 3. Fluxes of electrons, ions, and protons versus time during flyby C3. Different regions (magnetosphere, wake, disturbed region) are marked with different colors. The periodic signature when the energetic particles detector instrument looked into the corotational ion flow are depicted by arrows.

3 and 4 in Figure 5). In the wake there is also some higher energy isotropic background above 200 keV which sometimes indicate a peak energy around 900 keV (e.g., at 13:35 on day 309, 1996). Clearly the beams from the North are visible inside the wake for energies 15–29 keV and 55–83 keV as described before. For higher energies
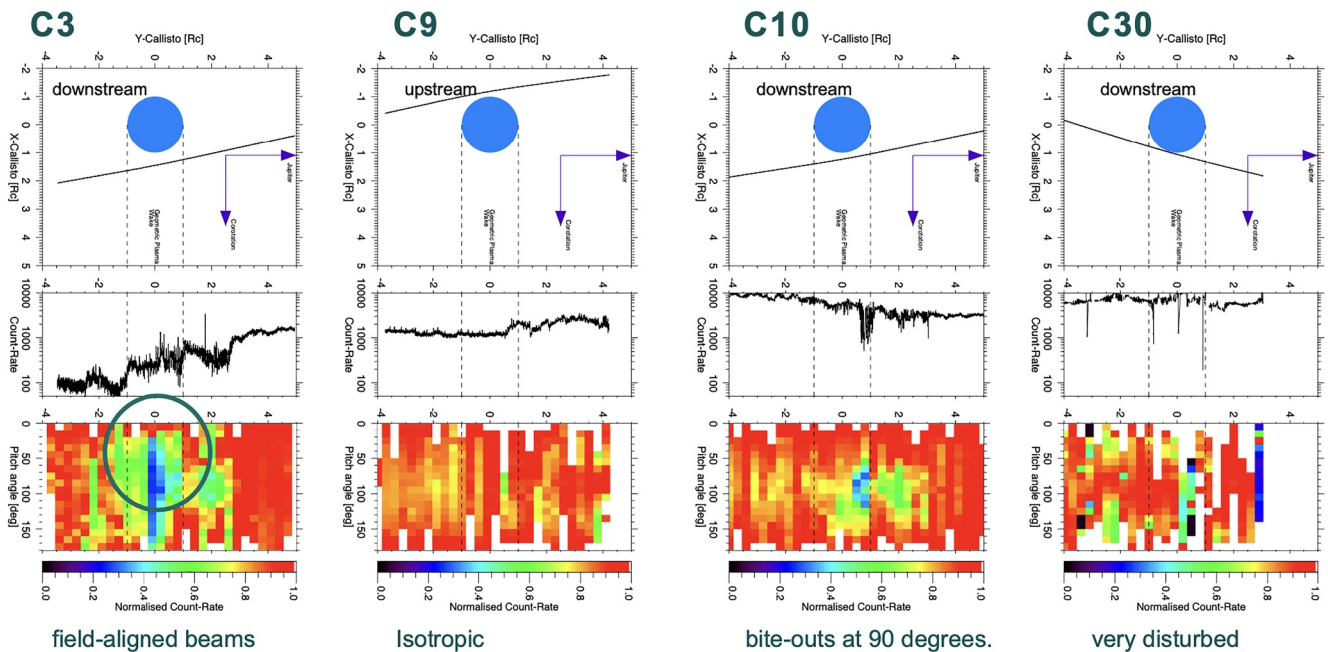
Figure 4. Count rates and normalized pitch angles of electrons (15–29 keV) during Callisto flybys C3, C9, C10, and C30 along the spacecraft trajectories in the *x*-*y*-plane of a Callisto centered coordinate system where x is in corotation direction and y is in the direction of Jupiter. The green circle in the bottom panel highlights the electron beams along the magnetic field direction.
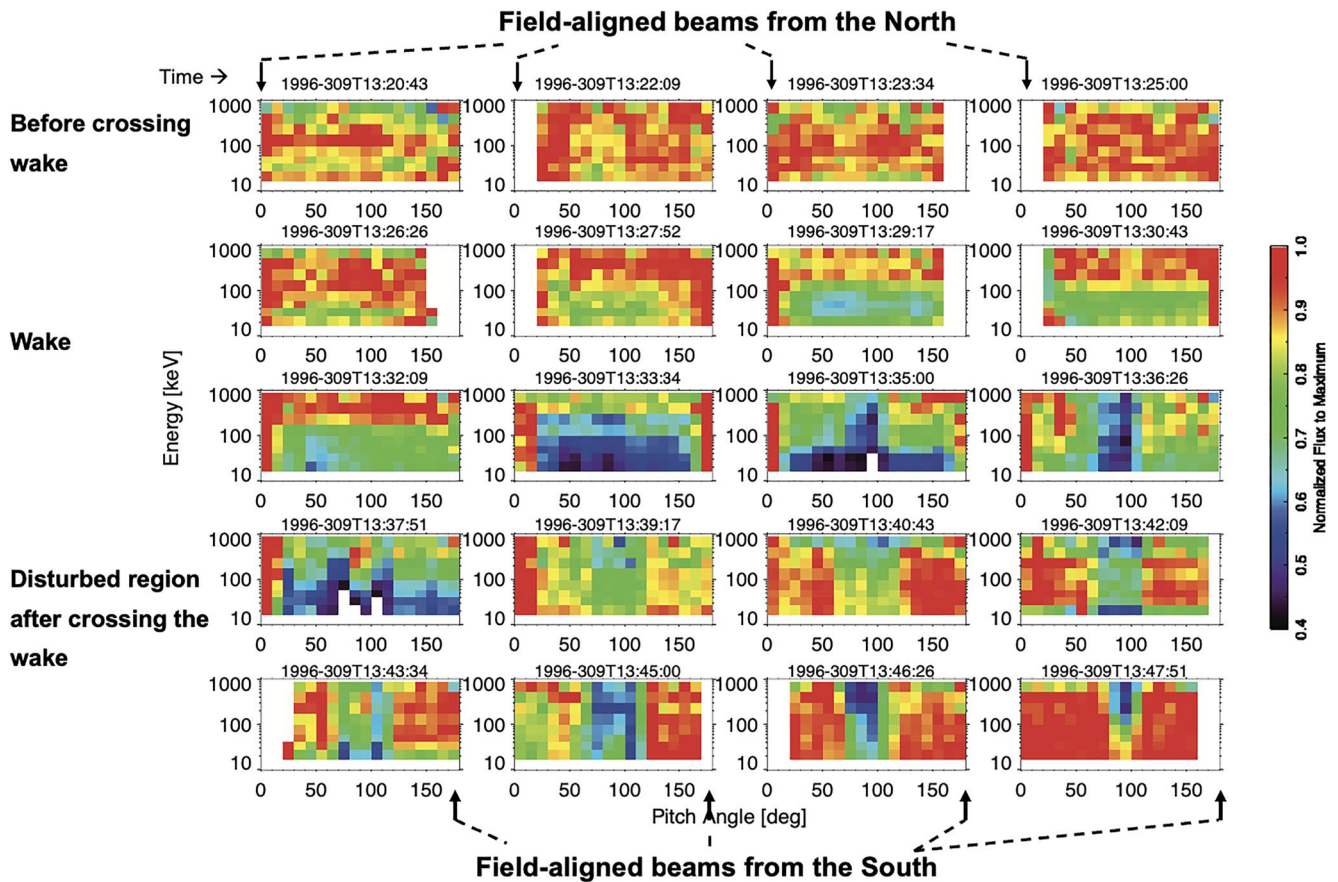
Figure 5. Energy versus pitch angle and color-coded normalized count rates of electrons for flyby C3 at individual times in separate boxes before the wake entry (upper and half of the second row), inside the wake (second half and third row and first box of row four), and inside disturbed region after crossing the wake (three last boxes in row four and entire row five). Field-aligned electron beams from the North appear at 0° pitch angles, beams from the South at 180°, respectively. Red is the maximum value, the minimum in dark blue or black is at 0.4 of the maximum value to increase contrast. Also, the colors are normalized to the maximum (1 = red) for each energy bin in each box independently.

the electron pitch angle distributions slightly change and the beams are less clear. Sharp dropout signatures around 90° pitch angle are noticeable up to 527 keV in the disturbed region before becoming nearly isotropic.

5. Pitch Angle Distribution of Energetic Ions Near Callisto

Figure 6 shows the corresponding ion plots (22–42 keV) in the same format as for electrons (15–29 keV) shown in Figure 4. For ions we first removed spikes in the data and then applied a smoothing and detrending of the count rates to remove the corotational effects but retaining the pitch angle variations as described in the previous section. The following Table 3 summarizes the used number of data points for different channels and flybys. The ± value indicates that using values increased or decreased by the given value did not change much the end result. The detrended rate is used to create the colored normalized pitch angle distributions in the lower panel. The normalization from 0 to 1 is done for each y-bin separately based on the max count rate. Flyby C3: before entry into the wake isotropic pitch angle distributions were observed. Inside the wake ion beams anti-parallel to the magnetic field direction from the South, also visible as spikes in the count rates, were clearly visible. At the entry into the wake the ion beam is quite sharp at 180° followed by a pitch angle distribution widening from beam-like to a distribution where all pitch angles between 90 and 180° show the same count rate. Shortly before the exit from the wake the pitch angle distribution reverses and show clear bite-out signatures between 90 and 150° pitch angle continued into the disturbed region outside the wake toward Jupiter. The periodic signature related to the look direction of the EPD sensor into the flow direction as described earlier is only seen outside the wake and only toward the planet while no such signatures are visible before entering the wake.

Flyby C9: Upstream of the moon the ion pitch angle distributions are nearly featureless or isotropic.
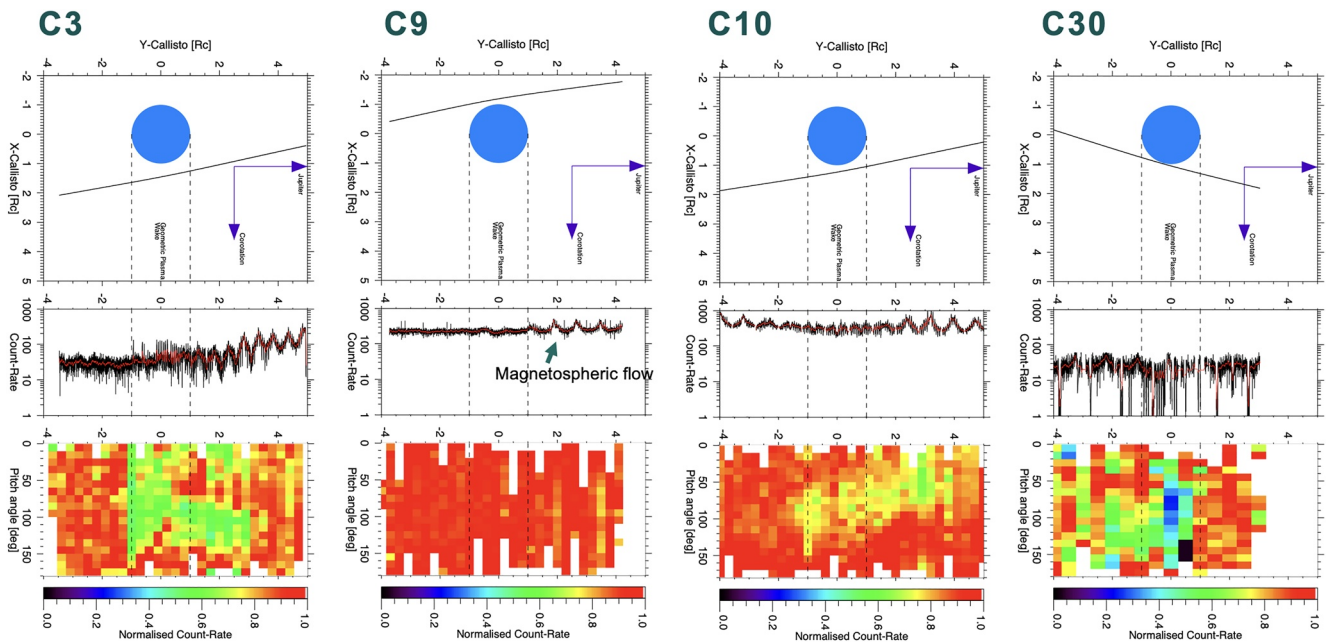
Figure 6. Count rates and normalized pitch angle of ions measured in channel A0 (22–42 keV) during Callisto flybys C3, C9, C10, and C30 along the spacecraft trajectories in the *x-y*-plane of a Callisto centered coordinate system. *X* is in corotation direction and y is in the direction of Jupiter. The *y*-axes are identical for all three panels. In the middle panel the actual count rate is shown in black and superimposed in red is a smoothed detrended profile removing mostly the corotation effects in the ion data. The lower panel shows the color-coded normalized pitch angle as a function of y using the detrended count rates.

Flyby C10: Before entering the wake the pitch angle distribution was isotropic. At the edge of and inside the wake there is 20% reduction for ions with 90° pitch angle. This reduction is slightly changing from 90 to 0° after exiting the wake toward Jupiter.

Flyby C30: The particle count rates close to the moon are very much disturbed and show sharp dropouts outside and also inside the wake. The spike removal procedure and the corresponding binning is less certain due to a worse statistics compared to the other flybys. Therefore, the binning in the *y*-direction has been doubled compared to the other flybys. Nevertheless, the resulting pitch angle distributions are not trustworthy enough to conclude anything.

For C3, C9, and C10 clear periodic variations in the count rates were visible caused by periodic measurements from the corotation direction predominantly after exiting the wake (or crossing the moon for flyby C9) toward the direction of Jupiter. For comparison, Figure 7 shows the pitch angle distributions of ions and protons (top panel) and electrons (bottom panel) with different energies measured during flyby C3. Clearly the electron beams from the North are visible at 0° pitch angle inside the wake for energies 15–29 keV and 55–83 keV as described before. For higher energies the electron pitch angle distributions slightly change and the beams are less clear. Sharp dropout signatures around 90° pitch angle are noticeable up to 527 keV in the disturbed region before becoming nearly isotropic. There is some evidence that the PAD minima at 90° in the disturbed region last longer for higher energies. The measurements in channel DC3 (>11,000 keV) show an overall trend of high fluxes at low pitch angles. This is pitch angle asymmetry, at least outside the wake for DC3, may be an artifact due to spacecraft obscuration of the DC3 FoV. Still, clearly the variations in the DC3 anisotropy in the wake show that there is a change in the angular distribution of the corresponding electrons. The deepest dropouts in that channel occur between 50 and 180° pitch angle in the same location as in the other electron channels. Pitch angle distributions of ions and protons are similar but also show minor differences. For all the energies we looked at we notice the change in the PAD minima from being 0–90 to 90–150° in the wake before exiting into the disturbed region. For channel A3 we find also counts at 0–90 while for channel A0 the count rates are very much reduced.

6. Discussion and Summary

We compared the results of flyby C3 with the output of a MHD simulation run from Seufert (2012) to put the data in a more general context and over the entire flyby. Figure 8 compares EPD measurements of electron intensities

GALILEO C3 (1996.309)
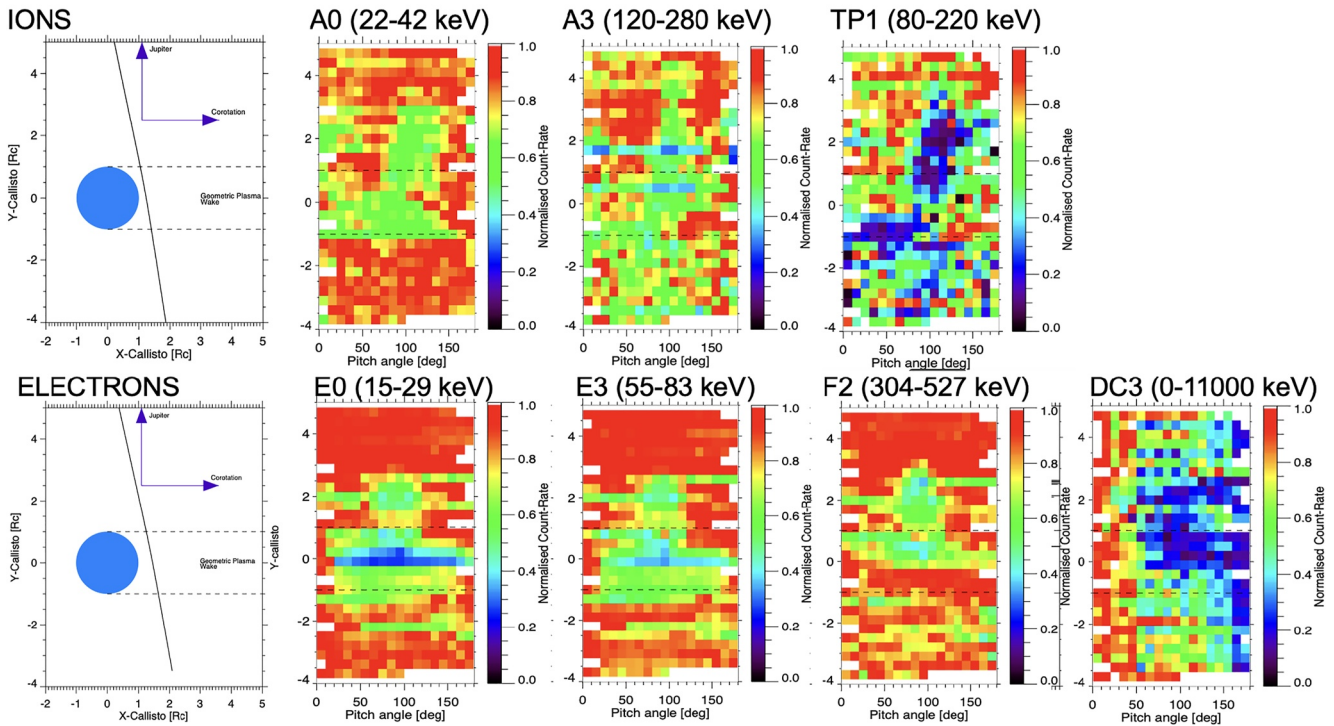
Figure 7. Pitch angle distributions during flyby C3 of ions and protons (top panel) and electrons (bottom panel) for different energies. The trajectory of the flyby is shown in the first column with Callisto in the center of the coordinate system. The dashed lines mark the geometric wake behind the moon. For ions the detrended pitch angle distributions are used as described before.

(15–29 keV), total magnetic field measurements of the MAG instrument, pitch angle distributions during flyby C3 with MHD simulations. In the simulation run the Alfvén-wing structure (Kivelson & Russell, 1995; Neubauer, 1980; Knight, 1973) is shown together with the trajectory of the flyby. Red marks part of the wake and the disturbed region described above. Please note that the geometric wake in the simulation is slightly inclined due to the individual setting of the run. It is expected that the electron beams occur in regions where the plasma flow/density and the magnetic field change and a current system builds up close to the moon. It was pointed out
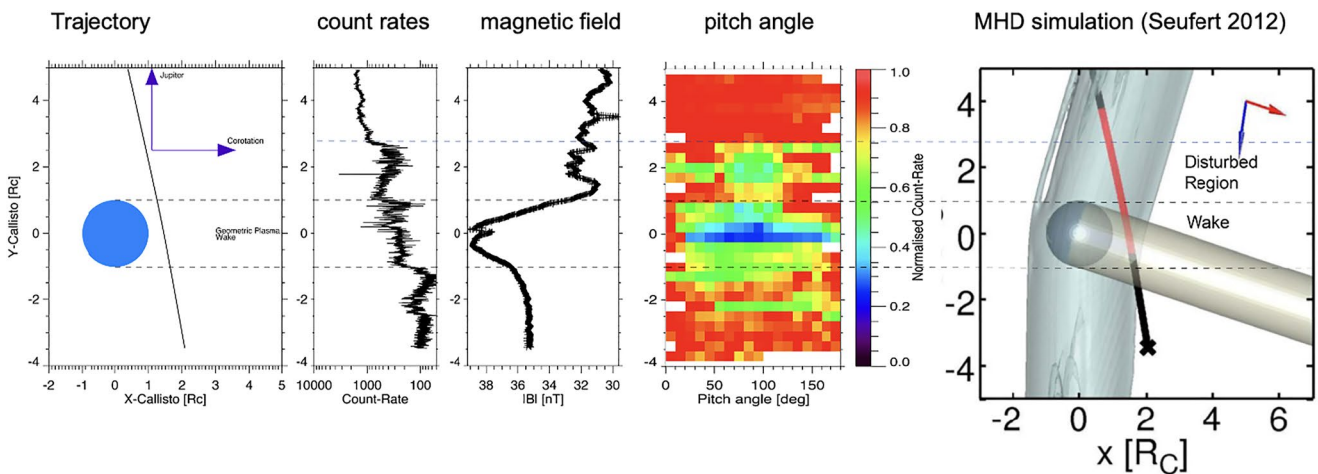
Figure 8. Comparison between measured electron fluxes, pitch angle distributions, measured magnetic field along the spacecraft trajectory of flyby C3 together with the results of a magnetohydrodynamic (MHD) simulation run by Seufert (2012). Dashed lines separate the nominal geometric plasma wake and the disturbed region outside the wake toward the planet. Note that in the MHD simulation the geometric wake is inclined due to the individual settings.

Table 3
Number of Data Points Used for the Detrending of the Ion Count Rates Before Calculating the Pitch Angles

Flyby	Channel	Number of data points
C3	A0	55 ± 7
C3	A3	27 ± 5
C3	TP1	27 ± 5
C9	A0	50 ± 7
C10	A0	70 ± 7
C30	A0	80 ± 7

by Jacobsen et al. (2010) that in order to maintain the current flow, electrons must be accelerated. The strongest electron beams were seen when the magnetic field was high in the center of the wake when the density of ions was low. There is also some evidence that the disturbed region (marked in red) corresponds to 90° dropouts in the pitch angle distributions. It looks like the spacecraft went through the Alfvén-wing structure with quite low, fluctuating total magnetic field. This is in accordance with the findings of Hess and Delamere (2012) near Io. They discussed the satellite-triggered planetary aurora caused by field-aligned electron beams between the ionosphere of a satellite and the planet and stated that the origin of the Alfvénic interaction is the satellite motion relative to the planetary magnetic field. Correlated accelerated electrons along the Io-Jupiter flux tubes were reported (Jones & Su, 2008). The electrons are accelerated in the opposite direction to the current direction (see Figure 1 of Khurana et al. (2007): on the $+y$ side the current is toward the moon while of the $-y$ location it is away from the moon). Therefore we sometimes find electron beams from the North, and sometimes from the South. The field-aligned acceleration can take place near Jupiter or near the satellite depending on where the lack of current carriers is. During flyby C3 the spacecraft enters the southern Alfvén-wing from the $-y$ direction at 13:20 where the current is flowing opposite to the field-aligned direction, that is, electrons would move in the direction of the magnetic field to close the current. Now we have evidence that also at Callisto Alfvén waves periodically could have accelerated electrons along the field lines up to several hundred keV and confirm the evidence first mentioned by Mauk and Saur (2007). Studies by Damiano et al. (2023), Coffin et al. (2022), and by Damiano et al. (2019) have explained accelerated field-aligned electrons observed by the Jade and Jedi instruments onboard the Juno spacecraft at high latitudes of the Jovian magnetosphere by broadband Alfvén waves at least in regions of the Io torus. We have now evidence that the same process might work at Callisto for energies up to several hundreds of keV. However, more detailed studies and simulations with Callisto-specific parameters are necessary to quantify and confirm those results. This should be the subject of a future study. The fact that we did not observe electron beams during the other wake flybys C10 and C30 may be explained by different environmental conditions near Callisto as compared to C3. The beams simply may have been further downstream as the flyby locations and were not detected onboard the Galileo spacecraft, dependent on one-way travel time of the Alfvén wave and the convection time of the plasma as mentioned by Jacobsen et al. (2010).

In summary, the findings of this paper are as follows:

1. Field-aligned electrons beams from the North and sometimes from the South up to several hundreds of keV during encounter C3 downstream of the moon were identified. C3 is the only downstream flyby where the spacecraft was at northern magnetic latitudes; no beams during encounters C9, C10, C30 have been observed when Galileo was on southern magnetic latitudes;
2. There is evidence for a disturbed interaction region outside the geometric wake toward Jupiter;
3. We observed bite-out region near 90° pitch angle in the geometric wake and in the disturbed region, sometimes short enhancements at 90° pitch angle;
4. The pitch angle distributions during upstream flyby C9 were nearly isotropic;
5. The magnetospheric flow of ions is significantly disturbed in the wake region and in the interaction (disturbed) region outside the wake;
6. A comparison of the observations with the simulation results from Seufert (2012) and Liuzzo et al. (2016) show similarities of a disturbed interaction region during flybys C3 and C10;
7. There is evidence that Alfvén waves might play a role in the acceleration of field-aligned electron beams near Callisto. Morace studies are needed to fully quantify and confirm this.

Data Availability Statement

In this study we used the updated calibrated data from the EPD (available through http://sd-www.jhuapl.edu/Galileo_EPD/ or in PDS: https://pds-ppi.igpp.ucla.edu/search/view/?f=yes&id=pds://PPI/galileo-epd-cal-corrected) and from the magnetometer instrument MAG onboard the Galileo spacecraft. All the used data sets are available and archived in the NASA PDS system.

References

Bagenal, F., Wilson, R. J., Siler, S., Paterson, W. R., & Kurth, W. S. (2016). Survey of Galileo plasma observations in Jupiter's plasma sheet. *Journal of Geophysical Research: Planets*, *121*(5), 871–894. https://doi.org/10.1002/2016JE005009

Bhattacharya, B., Thorne, R. M., Williams, D. J., Khurana, K. K., & Gurnett, D. A. (2005). Diffuse auroral precipitation in the Jovian upper atmosphere and magnetospheric electron flux variability. *Icarus*, *178*(2), 406–416. https://doi.org/10.1016/j.icarus.2005.06.013

Bhattacharyya, D., Clarke, J. T., Montgomery, J., Bonfond, B., Gérard, J.-C., & Grodent, D. (2018). Evidence for auroral emissions from Callisto's footprint in HST UV images. *Journal of Geophysical Research: Space Physics*, *123*(1), 364–373. https://doi.org/10.1002/2017JA024791

Coffin, D., Damiano, P., Delamere, P., Johnson, J., & Ng, C.-S. (2022). Broadband energization of superthermal electrons in Jupiter's inner magnetosphere. *Journal of Geophysical Research: Space Physics*, *127*(8), e30528. https://doi.org/10.1029/2022JA030528

Damiano, P. A., Delamere, P. A., Kim, E. H., Johnson, J. R., & Ng, C. S. (2023). Electron energization by inertial Alfvén waves in density depleted flux tubes at Jupiter. *Geophysical Research Letters*, *50*(5), e2022GL102467. https://doi.org/10.1029/2022GL102467

Damiano, P. A., Delamere, P. A., Stauffer, B., Ng, C. S., & Johnson, J. R. (2019). Kinetic simulations of electron acceleration by dispersive scale Alfvén waves in Jupiter's magnetosphere. *Geophysical Research Letters*, *46*(6), 3043–3051. https://doi.org/10.1029/2018GL081219

Frank, L. A., Ackerson, K. L., Lee, J. A., English, M. R., & Pickett, G. L. (1992). The plasma instrumentation for the Galileo Mission. *Space Science Reviews*, *60*(1–4), 283–304. https://doi.org/10.1007/bf00216858

Frank, L. A., & Paterson, W. R. (2002). Galileo observations of electron beams and thermal ions in Jupiter's magnetosphere and their relationship to the auroras. *Journal of Geophysical Research*, *107*(A12), 35–41. https://doi.org/10.1029/2001JA009150

Galli, A., Vorburger, A., Carberry Mogan, S. R., Roussos, E., Stenberg Wieser, G., Wurz, P., et al. (2022). Callisto's atmosphere and its space environment: Prospects for the particle environment package on board JUICE. *Earth and Space Science*, *9*(5), e02172. https://doi.org/10.1029/2021EA002172

Gurnett, D. A., Kurth, W. S., Roux, A., & Bolton, S. J. (1997). Absence of a magnetic-field signature in plasma wave observations at Callisto. *Nature*, *387*(6630), 261–262. https://doi.org/10.1038/387261a0

Gurnett, D. A., Persoon, A. M., Kurth, W. S., Roux, A., & Bolton, S. J. (2000). Plasma densities in the vicinity of Callisto from Galileo plasma wave observations. *Geophysical Research Letters*, *27*(13), 1867–1870. https://doi.org/10.1029/2000GL003751

Hess, S., & Delamere, P. A. (2012). Satellite-induced electron acceleration and related auroras. In *Auroral phenomenology and magnetospheric processes: Earth and other planets* (pp. 295–304). American Geophysical Union (AGU). https://doi.org/10.1029/2011GM001175

Jacobsen, S., Saur, J., Neubauer, F. M., Bonfond, B., Gérard, J. C., & Grodent, D. (2010). Location and spatial shape of electron beams in Io's wake. *Journal of Geophysical Research*, *115*(A4), A04205. https://doi.org/10.1029/2009JA014753

Jones, S. T., & Su, Y. J. (2008). Role of dispersive Alfvén waves in generating parallel electric fields along the Io-Jupiter fluxtube. *Journal of Geophysical Research*, *113*(A12), A12205. https://doi.org/10.1029/2008JA013512

Kane, M., Williams, D. J., Mauk, B. H., McEntire, R. W., & Roelof, E. C. (1999). Galileo energetic particles detector measurements of hot ions in the neutral sheet region of Jupiter's magnetodisk. *Geophysical Research Letters*, *26*(1), 5–8. https://doi.org/10.1029/1998GL900267

Khurana, K. K., Dougherty, M. K., Russell, C. T., & Leisner, J. S. (2007). Mass loading of Saturn's magnetosphere near Enceladus. *Journal of Geophysical Research*, *112*(A11), 8203. https://doi.org/10.1029/2006JA012110

Khurana, K. K., Kivelson, M. G., Stevenson, D. J., Schubert, G., Russell, C. T., Walker, R. J., & Polanskey, C. (1998). Induced magnetic fields as evidence for subsurface oceans in Europa and Callisto. *Nature*, *395*(6704), 777–780. https://doi.org/10.1038/27394

Khurana, K. K., Russell, C. T., & Dougherty, M. K. (2008). Magnetic portraits of Tethys and Rhea. *Icarus*, *193*(2), 465–474. https://doi.org/10.1016/j.icarus.2007.08.005

Kim, T. K., Ebert, R. W., Valek, P. W., Allegrini, F., McComas, D. J., Bagenal, F., et al. (2020). Survey of ion properties in Jupiter's plasma sheet: Juno JADE-I observations (Vol. *125*(4)). https://doi.org/10.1029/2019JA027696

Kivelson, M. G. (2004). Moon-magnetosphere interactions: A tutorial. *Advances in Space Research*, *33*(11), 2061–2077. https://doi.org/10.1016/j.asr.2003.08.042

Kivelson, M. G., Bagenal, F., Kurth, W. S., Neubauer, F. M., Paranicas, C., & Saur, J. (2004). Magnetospheric interactions with satellites. In F. Bagenal, T. E. Dowling, & W. B. McKinnon (Eds.), *Jupiter. The planet, satellites and magnetosphere* (Vol. 1, pp. 513–536).

Kivelson, M. G., Khurana, K. K., Means, J. D., Russell, C. T., & Snare, R. C. (1992). The Galileo magnetic field investigation. *Space Science Reviews*, *60*(1–4), 357–383. https://doi.org/10.1007/bf00216862

Kivelson, M. G., Khurana, K. K., Stevenson, D. J., Bennett, L., Joy, S., Russell, C. T., et al. (1999). Europa and Callisto: Induced or intrinsic fields in a periodically varying plasma environment. *Journal of Geophysical Research*, *104*(A3), 4609–4626. https://doi.org/10.1029/1998ja900095

Kivelson, M. G., & Russell, C. T. (1995). Introduction to space physics.

Kliore, A. J., Anabtawi, A., Herrera, R. G., Asmar, S. W., Nagy, A. F., Hinson, D. P., & Flasar, F. M. (2002). Ionosphere of Callisto from Galileo radio occultation observations. *Journal of Geophysical Research: Space Physics*, *107*(A11), 1407. https://doi.org/10.1029/2002JA009365

Knight, S. (1973). Parallel electric fields. *Planetary and Space Science*, *21*(5), 741–750. https://doi.org/10.1016/0032-0633(73)90093-7

Krupp, N., Lagg, A., Livi, S., Wilken, B., Woch, J., Roelof, E. C., & Williams, D. J. (2001). Global flows of energetic ions in Jupiter's equatorial plane: First-order approximation. *Journal of Geophysical Research*, *106*(A11), 26017–26032. https://doi.org/10.1029/2000JA900138

Lindkvist, J., Holmström, M., Khurana, K. K., Fatemi, S., & Barabash, S. (2015). Callisto plasma interactions: Hybrid modeling including induction by a subsurface ocean. *Journal of Geophysical Research: Space Physics*, *120*(6), 4877–4889. https://doi.org/10.1002/2015JA021212

Liuzzo, L., Feyerabend, M., Simon, S., & Motschmann, U. (2015). The impact of Callisto's atmosphere on its plasma interaction with the Jovian magnetosphere. *Journal of Geophysical Research: Space Physics*, *120*(11), 9401–9427. https://doi.org/10.1002/2015JA021792

Liuzzo, L., Simon, S., Feyerabend, M., & Motschmann, U. (2016). Disentangling plasma interaction and induction signatures at Callisto: The Galileo C10 flyby. *Journal of Geophysical Research: Space Physics*, *121*(9), 8677–8694. https://doi.org/10.1002/2016JA023236

Liuzzo, L., Simon, S., Feyerabend, M., & Motschmann, U. (2017). Magnetic signatures of plasma interaction and induction at Callisto: The Galileo C21, C22, C23, and C30 flybys. *Journal of Geophysical Research: Space Physics*, *122*(7), 7364–7386. https://doi.org/10.1002/2017JA024303

Liuzzo, L., Simon, S., & Regoli, L. (2019). Energetic ion dynamics near Callisto. *Planetary and Space Science*, *166*, 23–53. https://doi.org/10.1016/j.pss.2018.07.014

Mauk, B. H., & Saur, J. (2007). Equatorial electron beams and auroral structuring at Jupiter. *Journal of Geophysical Research*, *112*(A11), 10221. https://doi.org/10.1029/2007JA012370

Neubauer, F. M. (1980). Nonlinear standing Alfven wave current system at Io - Theory. *Journal of Geophysical Research*, *85*(A3), 1171–1178. https://doi.org/10.1029/JA085iA03p01171

Seufert, M. (2012). *Callisto: Induction signals, atmosphere and plasma interaction (Unpublished doctoral dissertation)*. Andreas Eckart University of Cologne.

Simon, S., Roussos, E., & Paty, C. (2015). The interaction between Saturn's moons and their plasma environments. *Physics Reports*, *602*, 1–65. https://doi.org/10.1016/j.physrep.2015.09.005

Tomás, A. T., Woch, J., Krupp, N., Lagg, A., Glassmeier, K.-H., & Kurth, W. S. (2004). Energetic electrons in the inner part of the Jovian magnetosphere and their relation to auroral emissions. *Journal of Geophysical Research*, *109*, 6203. https://doi.org/10.1029/2004JA010405

Waldrop, L. S., Roelof, E. C., & Fritz, T. A. (2015). Three-dimensional convective flows of energetic ions in Jupiter's equatorial magnetosphere. *Journal of Geophysical Research: Space Physics*, *120*(12), 10. https://doi.org/10.1002/2015JA021103

Williams, D. J., McEntire, R. W., Jaskulek, S., & Wilken, B. (1992). The Galileo energetic particles detector. *Space Science Reviews*, *60*(1–4), 385–412. https://doi.org/10.1007/bf00216863